Applied Mathematical Modelling 64 (2018) 265–284

Contents lists available at ScienceDirect

Applied Mathematical Modelling

journal homepage: www.elsevier.com/locate/apm

Modeling, simulation and optimization of general solar updraft towers

Hannes von Allwörden[a], Ingenuin Gasser[a,*], Muhammad Junaid Kamboh[b]

[a] Department Mathematik, Universität Hamburg, Bundesstraße 55, Hamburg 20146, Germany
[b] Institute of Micro System Technology, Hamburg University of Technology, Eißendorfer Straße 42 (M), Hamburg 21073, Germany

ARTICLE INFO

Article history:
Received 4 October 2017
Revised 2 July 2018
Accepted 11 July 2018
Available online 20 July 2018

Keywords:
Solar updraft tower
Sloped collector field
Humidity
Small Mach number

ABSTRACT

A model to describe a solar chimney power plant with a generally sloped collector field and for the general situation of humid air is presented. This is a significant development of existing simple models for solar updraft towers with planar collector fields for the situation of purely dry air. The model describing the gas dynamics in the collector and in the chimney includes a turbine model, friction and heat transfer losses, evaporation and condensation models etc. However, the relevant physics can be modeled in one space dimension. It is the result of a fully compressible gas dynamic model in the small Mach number limit. A numerical algorithm is defined which admits very fast simulations. Therefore optimization procedures can easily be applied. Numerical results on optimization with respect to geometric and physical parameters which may be considered both in the planning and the operational phase are presented. The results are compared qualitatively and – if available – quantitatively to prototype data and to simulations from the literature.

1. Introduction

The global demand for electrical energy continues to grow due to increasing global population and industrialization. On the other hand, the mineral resources e.g. oil, natural gas, and coal, on which we have traditionally relied to produce electricity, are depleting. This is only one of the reasons that the prices of these resources are rising. In addition, nowadays, environmental concerns like emissions and greenhouse effect, safety and health hazards pertaining to electricity production are becoming more important, particularly in the highly industrialized countries. Numerous examples of disasters related to nuclear energy have been witnessed, the most recent of them being at Fukushima, Japan 2011. Therefore, sustainable and environment friendly methods to produce electricity are gaining more and more importance. Developed countries around the world are devoting more and more special efforts to this challenge.

The focus of this study is to analyze so called “solar chimney power plants with sloped collectors” which are based on the solar thermal principle. The idea has been pioneered by Bilgen and Rheault in [1] and originated as an offspring of so called “solar updraft towers” (SUT). For an overview on SUTs see [2–6].

* Corresponding author.
E-mail address: ingenuin.gasser@uni-hamburg.de (I. Gasser).

https://doi.org/10.1016/j.apm.2018.07.023

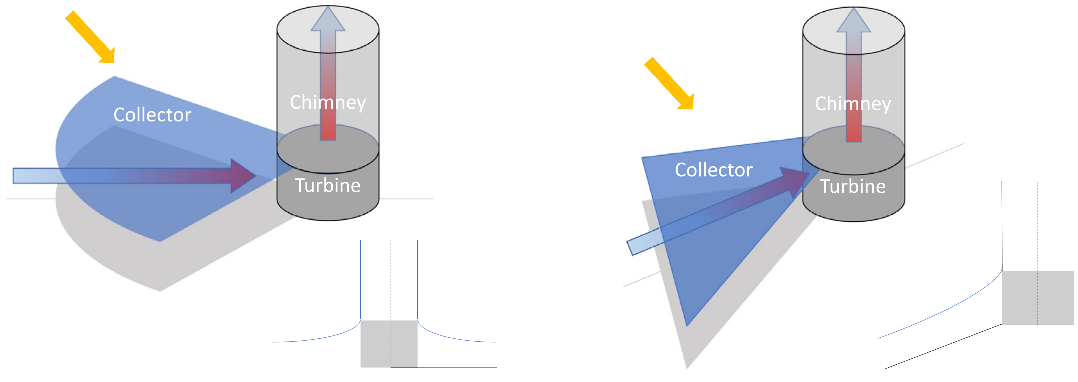

(a) Principle of a Solar Updraft Tower with horizontal collector

(b) Plant with sloped collector field and small chimney at the top, as proposed by [1]

Fig. 1. General design of solar updraft towers.

The SUT consists of three components, namely collector, chimney, and a turbine. The collector section is like a roof made up of glass or some transparent material which stands at a few meters height from the ground. A high vertical chimney stands in the center of the collector section, or, in case of a sloped collector field, at its uphill end. A turbine is installed at the bottom of the chimney where it meets the collector. The power plant operates on two well-known physical phenomena, i.e. the greenhouse effect and the chimney effect. The air inside the collector is heated up due to greenhouse effect as the solar radiation falls on the glass roof. The less dense heated air tends to rise up due to buoyancy forces and therefore a flow of air is generated towards the chimney. This resulting air flow drives the turbine. Clearly, the output increases heightening chimney and enlarging the collector area. See Fig. 1 for components and working principle of a solar updraft tower.

In this paper we discuss two important issues regarding extended modeling and applications of SUTs. One is a variant proposed in [1] to consider mountainous regions. The second issue is to generalize the model to the situation of humid air in order to understand the possible influences of humidity on the performance.

Let us start with the possibility of mountainous regions. This implies building a collector field along the slope of a mountain or a hill which then also functions as chimney such that on top only a smaller vertical chimney is needed. As an example we can imagine a triangular collector area on a hill directed versus south. See Fig. 1(b) for the working principle for such a solar chimney power plant. This variant has big advantages. On one side the construction costs for the (smaller) chimney are much lower and on the other side – suppose the direction of the collector field is appropriately chosen versus south – the angle of incidence of the radiation on the collector field (depending on the latitude) is higher and therefore a higher output of power is obtained. In addition in many regions it is easier to find hills or mountains instead of large flat areas (as it is needed for the classical variant of the solar updraft tower). Therefore this idea was proposed in particular for mountainous areas at higher latitude [1].

Now let us come to the issue of humid air. Considering the temperature range the air experiences on its way through the plant and its influence on the material properties, it is natural to ask how water vapor affects the operation of a SUT by condensation and evaporation. This is done by Kröger and Blaine in [7], where it is found that “moist air generally improves the draft and that condensation may occur in the chimney under certain conditions”. The paper does, however, only consider the chimney, i.e the different amounts of energy needed for heating and evaporation in the collector are not accounted for.

Therefore the influence of humidity for the whole power plant is not yet studied and not obvious. Most models neglect water vapour completely for the sake of simplicity. The usual argument for the restriction to dry models is the assumption that typical areas of operation, e.g. deserts, would be highly arid. On the other hand, especially here the recovery of condensated water could be a desirable side-effect, making plants more cost effective. To this end, several variations to use SUTs for sea water desalination have been proposed, either adding closed stills to the collector ground [8,9] or attempting to re-gain water vapour at the top of the chimney by a high-efficiency condenser [10].

Given its enormous area demand, agricultural use of parts of the collector is desirable. In his dissertation, Pretorius investigates the role of evapotranspiration in an elaborate model and finds the potential power production lowered significantly compared to classic conditions [11].

The idea of this paper is to model, simulate and to optimize a Solar Updraft Tower with sloped collector in the general situation of humid air. The main focus is on using a model which allows very fast simulations such that optimization (i.e. with respect to certain parameters) can easily be done. In Section 3 the model is presented, in Section 3.5 the crucial small Mach number asymptotics is explained, in Section 4 different numerical schemes are proposed and tested, and in Section 5 the related optimizations with respect to certain parameters are performed.

We summarize the main features of the model:

- The model is derived from the fully compressible fluid dynamic equations.
- The small Mach number is used to simplify the model.
- There are no assumptions on the density or the temperature profiles in the collector or the chimney.
- Here the core is the fluid dynamic part, in [1] the attention is mainly given to the thermal transfer model.
- It is a continuous time dependent model. With this it allows transient simulations and we obtain automatically the stable stationary solutions (as long time behavior).
- It is easy to include time dependencies in the data, e.g. a daily radiation profile. With this it is easy to simulate a (longer) time period and to average over it.
- For even faster simulations, the steady state system can be considered. For many questions the stationary solution contains sufficient information.
- We apply the model to (easily) optimize the power output.

2. History and model evolution

In the context of renewable and sustainable energies, over the years a multitude of proposals have been made. As with any technology, there is never ending room for improvement and innovation in this field. However, very special consideration is being given to electrical energy production from solar radiation, the reason being simply that the solar radiation is virtually infinite over time. Moreover, there are several regions where sunlight is readily available in quantitatively acceptable levels of power density, particularly desert areas.

Currently there are two main approaches to produce electricity from solar radiation: The photovoltaic technology, converting radiation directly into electrical current, and the solar thermal technology, converting solar energy into electrical energy indirectly. The solar updraft tower technology considered in this paper is a solar thermal power plant.

Historically, the concept of solar updraft towers has been around for over a century now. One of the earliest descriptions of the solar chimney concept was presented by Spanish Colonel Isidoro Cabanyes in 1903 [12], for more details, also see [13]. In 1926, French Engineer Bernard Dubos proposed a solar chimney plant with its chimney resting on a mountain slope [3]. In 1931, the German Hanns Günther illustrated such a solar power plant more concretely [14]. Some pictures of each of these proposals can be found in [3]. Finally, the first experimental prototype of a solar updraft tower on an "industrial" scale was constructed at Manzanares, Ciudad Real, Spain in 1982. The project was funded by German government and supervised by Jörg Schlaich [5,15,16]. However, there have been built many other smaller prototypes in the last decades [17–19].

Solar updraft towers have certain merits which make them worth considering and comparable to other renewable energy proposals at present. No sophisticated technology is involved, it is almost free of deterioration, their operation and maintenance costs are low and the technology permits to work even over decades. However, for a full scale commercial power plant to have desirable power output, large land area is required for the collector field and construction of a high chimney can lead to civil engineering problems and therefore high costs [20,21]. The associated problems can be solved to a reasonable extent. Nevertheless, the technology is in direct competition with the hightech photovoltaic technology and other solar thermal approaches. Apart from the already mentioned advantages, the solar updraft technology has the possibility to store (again in a lowtech manner) a part of the absorbed energy over the range of up to a day. This is done by installing a water storage system in the collector ground which absorbs energy (heat) during the day and releases it during the night to maintain continuous (non-constant) supply of electrical energy [2].

There are many variants and ideas around this technology. For an overview see [22,23].

A somehow related idea, based on an inverted downward flow, is the so called energy tower. There the energy production originates in the evaporation energy of the employed water (see [24,25] for details). This is important because for the energy tower a detailed description of the humidity and the evaporation is needed.

Apart from the ones mentioned before there are papers concerning the modeling approaches to study solar updraft towers from a range of different perspectives. Some papers concern specific (modeling) questions related to the collector [26,27], the chimney [7,28–30], the turbine [31] or the power output [32]. In the literature which considers the full power plant there are some approaches which do significant simplifications, i.e. no losses in the energy balance [17,18,33,34], linear density profiles [1], stationary conditions only [35,36] etc. Other papers focus on full 3 dimensional fluid dynamic simulations of the air flow in a Solar Updraft Tower [37,38]. These are clearly very expensive simulations and not appropriate for fast optimization issues. Generally we can conclude that there is still a need for reasonably complex models, which adequately describe the physical features of the system, permit fast simulations, and allow for optimization procedures. In the context of solar chimney power plants with sloped collectors, there is almost no literature except the fundamental idea in [1].

3. Modeling

In this section, we explain how the basic model introduced in [39] for a SUT with flat collector and dry air can be extended to account for the general setting of sloped collector fields and condensation or evaporation on surfaces. In addition we explore further possible refinements and simplifications in the approach. One is to consider the collector-turbine-chimney unit as a simple network. The other one is the use of the steady state equations for describing the quasi-stationary situation where changes in the external data (radiation, outside temperature etc.) occur on a slow time scale.

In Section 3.1 we set up the 2d Euler equations for wet air in a SUT with a very general geometry. The corresponding initial and boundary conditions are discussed in Sections 3.2 and 3.3, respectively. By integration perpendicular to the main air movement, we obtain a 1d model in Section 3.4, where source and sink terms for evaporation and condensation arise from the surface boundary conditions. This model is further simplified in Section 3.5 and the steady state equations are considered in Section 3.6.

The experimental data from the Manzanares prototype [15,16] show that the temperature rise in the collector is approximately around 20 Kelvins and the flow velocities are of order 10 m/s [2]. Comparable values are obtained in [1] for the case of power plants with sloped collector, and in [35] and [7] for SUTs with humidity.

In light of the small velocities (compared to the speed of sound), we have to deal with a small Mach number flow and a compressible model seems not to be suitable, an incompressible model might seem appealing. But on the other hand, the chimney effect is based on density changes and therefore the flow cannot be treated as incompressible. The fact that the flow is driven by buoyancy forces as a result of small density changes may point to the possibility of using the Boussinesq approximation [40]. There are examples where the Boussinesq approximation is proved not to work well, i.e. in the case of a simple chimney with fire as a heat source [41]. We do not generally exclude the possibility of using the Boussinesq approximation for solar updraft towers, but here we use a more general approach. The small Mach number approach we choose in this paper allows us to identify whether the typical features of the Boussinesq approximation – linear profiles in pressure, density and temperature – are confirmed by simulations or not. In this sense we reduce the uncertainness introduced by using an approximative model like the Boussinesq approximation. Similar considerations concerning small Mach number approximations are discussed in [30] in case of high chimneys.

The aim of this study is to present a simple one-dimensional model to describe gas/air dynamics inside the power plant with sloped collector field and humidity. A typical air particle enters the collector section, travels through the turbine and leaves the system at the top of chimney. The particle path can be considered as one spatial dimension in modeling analysis. The cross sectional area perpendicular to the particle path is rectangular in the collector opening which becomes, assuming constant roof height, linearly small and eventually becomes constant and circular in the chimney due to constant radius. This one dimensional approach was already used successfully in [39] to model the simplest case with completely dry air and a flat collector. There is no indication that multidimensional effects are crucial (or cannot be modeled in the one dimensional approach). Moreover, a one dimensional model has many significant advantages with respect to a multidimensional approach. The model presented in [39] considers the full power plant and is aimed to permit very fast numerical simulations. This is necessary to be applied for optimising a power plant with respect to parameters or in the operational phase.

3.1. 2d Euler equations

We assume the SUT to be symmetric to its center axis and the flow to have no angular component. Therefore we can denote the position of a particle within the plant in cylinder coordinates by $(\tilde{r}, \tilde{h})$. While the chimney is assumed to have a cylindrical shape for simplification, we have more freedom of choice in the collector, as long as all "typical" particle trajectories remain comparable. This allows for the deviation from strictly cylindrical collectors e.g. to (not necessarily linear) "funnel" approaches suitable for sloped collectors or for a modification of the collector roof profile in order to address the change of density resulting from the cross-sectional change. In this manner, we can describe a variety of possible collector geometries. For instance, the collector length L_{coll} is to be understood as the arc length of the typical particle path, i.e. the collector radius in the case of a planar circular collector, or the triangle height in the case of an isosceles triangle.

Collector and chimney are coupled by an inner "box" in which the air is guided from horizontal to vertical motion and energy is extracted by one or more turbines (see Fig. 2(a) for general model geometry nomenclature).

The air in collector and chimney can be described by the well-known 2d Euler equations on a cylinder for a mixture of dry air and water vapour with molar amounts $\tilde{n}_{\mathrm{a}}, \tilde{n}_{\mathrm{h}}$, respectively, on the domain $\Omega = \Omega_{\mathrm{coll}} \cup \Omega_{\mathrm{chim}}$ (see Fig. 2(a)). As usual, unscaled quantities are denoted by tildas. The Euler equations are a set of four balance equations and an additional closing relation for the five unknowns $\tilde{n}_{\mathrm{a}}$, $\tilde{n}_{\mathrm{h}}$, velocity u, pressure $\tilde{p}$, and temperature $\tilde{T}$:

$$\frac{\mathrm{D}}{\mathrm{D}\tilde{t}}(\tilde{r}\tilde{n}) = 0 \tag{1a}$$

$$\frac{\mathrm{D}}{\mathrm{D}\tilde{t}}(\tilde{r}\tilde{n}_{\mathrm{h}}) - \tilde{\nabla}\left(D\tilde{n}\tilde{r}\tilde{\nabla}\left(\frac{\tilde{n}_{\mathrm{h}}}{\tilde{n}}\right)\right) = 0 \tag{1b}$$

$$\frac{\mathrm{D}}{\mathrm{D}\tilde{t}}(\tilde{r}\tilde{\rho}\tilde{u}) + \tilde{r}\tilde{\nabla}\tilde{p} - g\tilde{r}\tilde{\rho} - \mu\left(\tilde{\nabla}\left(\tilde{r}\tilde{\nabla}\tilde{u}\right) + \frac{1}{3}\tilde{\nabla}^2(\tilde{r}\tilde{u})\right) = 0 \tag{1c}$$

$$\frac{\mathrm{D}}{\mathrm{D}\tilde{t}}\left(\tilde{r}\tilde{\rho}\left(c\tilde{T} + \tilde{u}^2/2 + \tilde{h}g\right)\right) + \tilde{\nabla}(\tilde{r}\tilde{p}\tilde{u}) - \tilde{\nabla}\left(k\tilde{\nabla}\tilde{T}\right) = 0 \tag{1d}$$

$$R\tilde{T}(\tilde{n}_{\mathrm{a}} + \tilde{n}_{\mathrm{h}}) = \tilde{p}. \tag{1e}$$

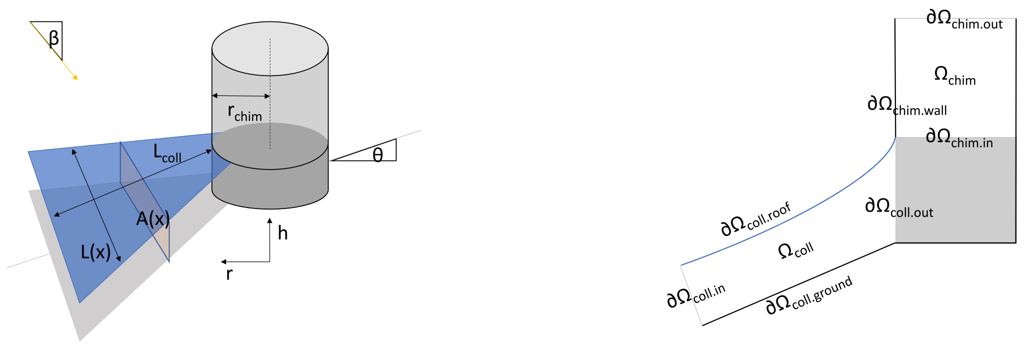

(a) Nomenclature for geometric parameters

(b) Nomenclature for domains and boundaries

Fig. 2. Nomenclature.

Table 1
Derived variables.

Symbol	Definition	Meaning
$\tilde{n}$	$\tilde{n}_a + \tilde{n}_h$	Molar amount of wet air
$\tilde{\rho}$	$M_a\tilde{n}_a + M_h\tilde{n}_h$	Mass density
c	$(c_a\tilde{n}_a + c_h\tilde{n}_h)/\tilde{n}$	Spec. heat capacity of wet air

Table 2
Operators.

Symbol	Definition
$\tilde{\nabla}$	$\begin{pmatrix} \partial/\partial\tilde{r} \\ \partial/\partial\tilde{h} \end{pmatrix}$
$\frac{\mathrm{D}}{\mathrm{D}\tilde{t}}$	$\partial/\partial\tilde{t} + \tilde{u}\tilde{\nabla}$

Table 3
Fixed parameters.

Symbol	Dimension	Value	Meaning
M_a	M^1N^{-1}	0.0289 kg/mol	Molar mass of dry air
M_h	M^1N^{-1}	0.018 kg/mol	Molar mass of water
D	L^2T^{-1}	$2.3 \cdot 10^{-5}$ m^2/s	Diffusion coefficient water vapour - air
g	L^1T^{-2}	9.81 m/s^2	Gravitational acceleration
μ	$M^1L^{-1}T^{-1}$	$17.1 \cdot 10^{-6}$ Pa s	Dynamic viscosity of dry air
c_a	$L^2T^{-2}\theta^{-2}$	718 J/(kg K)	Specific heat capacity of dry air
c_h	$L^2T^{-2}\theta^{-1}$	1556 J/(kg K)	Specific heat capacity of water
k	$M^1L^1T^{-3}\theta^{-1}$	0.0262 W/(m K)	Thermal conductivity of dry (!) air
R	$M^1L^2T^{-2}N^{-1}\theta^{-1}$	8.314 J/(mol K)	Gas constant

The newly introduced variables, operators and parameters are explained in Tables 1, 2, and 3, respectively. After scaling, we obtain

$$\frac{\mathrm{D}}{\mathrm{Dt}}(rn) = 0 \tag{2a}$$

$$\frac{\mathrm{D}}{\mathrm{Dt}}(rn_h) - \Gamma\nabla\left(rn\nabla\left(\frac{n_h}{n}\right)\right) = 0 \tag{2b}$$

$$\frac{\mathrm{D}}{\mathrm{Dt}}(r\rho u) + \frac{1}{\epsilon}r\nabla p - \frac{e_2}{\mathrm{Fr}^2}r\rho - \frac{1}{\mathrm{Re}}\left(\nabla(r\nabla u) + \frac{1}{3}\nabla^2(ru)\right) = 0 \tag{2c}$$

$$\frac{\mathrm{D}}{\mathrm{Dt}}\left(r\left((c_1n_h + n_a)T + (\gamma-1)\epsilon\rho\frac{u^2}{2} + (\gamma-1)\frac{\epsilon}{\mathrm{Fr}^2}\rho h\right)\right) + (\gamma-1)\nabla(rup) - \nabla\left(r\frac{\mathrm{Re}}{\mathrm{Pr}}\nabla T\right) = 0 \tag{2d}$$

Table 4
Reference values for Manzanares test plant.

Symbol	Dimension	Value	Interpretation
l_r	L^1	320 m	Collector length+chimney height
u_r	L^1T^{-1}	10 m/s	Typical gas velocity at turbine
p_r	$M^1L^{-1}T^{-2}$	101328 Pa	Typical pressure at ground level
T_r	θ^1	300 K	Typical temperature at ground level

Table 5
Dimensionless numbers.

Symbol	Definition	Value	Name
Γ	$\frac{D}{l_\mathrm{r}u_\mathrm{r}}$	$7.54\cdot10^{-9}$	Diffusion coefficient
$\frac{1}{\epsilon}\left(=\frac{1}{\gamma\mathrm{Ma}^2}\right)$	$\frac{p_\mathrm{r}}{u_\mathrm{r}^2\rho_\mathrm{r}}$	861	related to Mach number
$\frac{1}{\mathrm{Fr}^2}$	$\frac{gl_\mathrm{r}}{u_\mathrm{r}^2}$	29.9	Froude number
$\frac{1}{\mathrm{Re}}$	$\frac{\mu}{l_\mathrm{r}u_\mathrm{r}\rho_\mathrm{r}}$	$2.09\cdot10^{8}$	Reynolds number
$(\gamma-1)$	$\frac{R}{c_\mathrm{a}}$	0.29	Adiabatic exponent (dry)
$\frac{\mathrm{Re}}{\mathrm{Pr}}$	$\frac{k}{u_\mathrm{r}c_\mathrm{a}\rho_\mathrm{r}l_\mathrm{r}}$	$7.27\cdot10^{-9}$	Reynolds over Prandtl number
c_1	$\frac{c_\mathrm{h}M_\mathrm{h}}{c_\mathrm{a}M_\mathrm{a}}$	1.28	quotient of specific heat capacities
c_2	$\frac{M_\mathrm{h}}{M_\mathrm{a}}$	0.62	quotient of molar masses

$$nT \;= p \tag{2e}$$

where the reference values for scaling and the definitions and values of the dimensionless numbers can be found in Tables 4 and 5. Note that the given values refer to the Manzanares test plant and will vary for some of the examples considered later. Of course, (2a) or (2b) could be replaced by an analogous equation for n_a.

Let us make a few comments on the modeling of condensation phenomena. We assume that surface condensation/evaporation is of particular importance because of the cooled chimney walls and the high available surface area, especially for comparably small chimney radii. Therefore general condensation mechanisms such as droplets inside the air stream are assumed to be of lower relevance and to become important only for higher values of humidity which are not of particular interest for SUTs. Thus potential condensation energy carried by n_h can be neglected in energy conservation (2d) and our model by design cannot show precipitation effects inside the chimney as predicted by Kröger and Blaine [7].

Droplet condensation in SUTs has been considered in [42]. In our model it could be incorporated by appropriate source and sink terms and additional conservation laws. We refrain from doing so due to the mentioned arguments and in favor of model simplicity, although we cannot completely rule out the forming of clouds in the chimney. A comparable model for down-draft "energy towers" including evaporation from droplets instead of films has been proposed in [25]. Further ideas for the implementation of droplets can be found in [43,44].

3.2. Initial conditions

For transient simulations, we have to prescribe appropriate initial conditions in $t=0$ for the unknowns n_a, n_h, T, u, and p. Note that, because of relation (2e), only four conditions have to be specified. A natural choice are the profiles for temperature, pressure and density given in the surrounding atmosphere. These profiles vary very much depending on the circumstances. For consistency, we choose the adiabatic atmosphere formulas obtained by solving a stationary version of (2a)–(2d) as shown in [39].

3.3. Boundary conditions

We now impose boundary conditions for the solid surfaces, i.e. chimney walls $\partial\Omega_{\mathrm{chim.wall}}$, collector roof $\partial\Omega_{\mathrm{coll.roof}}$ and -ground $\partial\Omega_{\mathrm{coll.ground}}$ (see Fig. 2(a)):

$$u_\perp := \vec{n}(\vec{n}\cdot\vec{u}) = \vec{u} \tag{3a}$$

$$n_\mathrm{h} = n_\mathrm{h}^{\mathrm{sat}} := \frac{1}{T}\exp\left(11.96 - \frac{3984}{T\frac{T_\mathrm{r}}{1\,\mathrm{K}} - 38.15}\right)\frac{1\,\mathrm{bar}}{p_\mathrm{r}} \tag{3b}$$

$$J_\mathrm{a} \;:=\; n_\mathrm{a}u_\perp - \Gamma n\frac{\partial}{\partial\vec{n}}\left(\frac{n_\mathrm{a}}{n}\right) = 0 \tag{3c}$$

Table 6
Parameters.

Symbol	Value	Meaning
h	43900 J/mol	Enthalpy of vaporization
$\tilde{\alpha}$	$10\,\mathrm{W/(m^2\,K)}$	Heat transfer coefficient
$\tilde{q}$	$0.3 \cdot 10^3\,\mathrm{W/m^2}$	Solar radiation energy

Table 7
Dimensionless numbers.

Symbol	Definition	Value
$\frac{1}{\mathrm{Ja}}$	$\frac{hn_\mathrm{r}}{c_\mathrm{a}\rho_\mathrm{r}T_\mathrm{r}}$	5.03
α	$\frac{\tilde{\alpha}t_\mathrm{r}}{c_\mathrm{a}\rho_\mathrm{r}l_\mathrm{r}}$	$1.14 \cdot 10^{-3}$
Q	$\frac{\tilde{q}t_\mathrm{r}}{c_\mathrm{a}\rho_\mathrm{r}l_\mathrm{r}T_\mathrm{r}}$	$1.14 \cdot 10^{-4}$

$$\frac{\partial T}{\partial \vec{n}} = \frac{1}{\mathrm{Ja}}\frac{\mathrm{Pr}}{\mathrm{Re}}J_\mathrm{h} - \begin{cases} \alpha\,(T_\mathrm{ex} - T) & \text{on } \partial\Omega_\mathrm{chim.wall} \cup \partial\Omega_\mathrm{coll.roof} \\ Q\cos\,(\theta - \beta) & \text{on } \partial\Omega_\mathrm{coll.ground}, \end{cases} \tag{3d}$$

where the new parameters and dimensionless numbers are given in Tables 6 and 7.

Condition (3a) represents the usual no-slip condition. If condensation or evaporation occurs, there will be at least a thin layer of liquid water on the surfaces, saturating the air in the vicinity with water vapour. We assume that during operation, the surfaces are drained where necessary so that the plant is not flooded and the water layer remains thin, not affecting thermal conductivity etc. The parametrization of saturation vapour pressure by the Antoine equation in (3b) was taken from [45]. In (3c) we express the assumption that the dry portion of the air cannot pass through walls, whereas we will have negative J_h for condensation and positive J_h for evaporation. Due to this unambiguousness, we will write J instead of J_h. The Robin-type condition (3d) represents Newton's cooling law, complemented by the term $\frac{1}{\mathrm{Ja}}\frac{\mathrm{Pr}}{\mathrm{Re}}J$ representing released or absorbed condensation energy. For the collector roof and chimney wall, the heat transfer coefficient $\tilde{\alpha}$ models both heat conduction through the material and the (wind-dependent) transfer to the ambient air.

The solar radiation is given by Q. It enters through the collector ground, because most of the solar energy is absorbed by the ground and transferred to the air convectively (note that the imposed initial condition does not account for this). This allocation of the heat source turns out to be crucial for the calculation of evaporation rates. Of course, Q is a function of time and could be enhanced – if known and available – with factors for spatial dependent shading, reflectivity, etc. For simplicity and due to lack of available data we assume Q only to be time dependent. Since Q changes only slowly and significantly only on a timescale of hours, for many of our short time simulations Q does not even change in time. But there is no difficulty to include its time dependence when running simulations over many hours.

We resign from establishing a more elaborate time-dependent heat transition model, i.e. incorporating time- and spatial dependent submodels for Q and α, or more sophisticated setups including e.g. water bags or multiple glazing. These are described in detail in [11] and [35] and could easily be integrated, but do not lie in the focus of this work.

Next, we model the transition from the collector outlet to the chimney entrance. The SUT can be regarded as a system of coupled pipes, suggesting a treatment similar to [46]. The turbine section is treated as a "black box" instead of trying to precisely model the streamlines inside by means of balance equations. These connect the values integrated over chimney entrance $\partial\Omega_\mathrm{chim.in}$ and collector exit $\partial\Omega_\mathrm{coll.out}$ with area $A_\mathrm{coll.out}$. The resulting time delay is neglected.

$$\int_{\partial\Omega_\mathrm{coll.out}} rf(\vec{x})\,\mathrm{d}\vec{x} = \int_{\partial\Omega_\mathrm{chim.in}} rf(\vec{x})\,\mathrm{d}\vec{x} \quad \forall f \in \{T, n, \rho, n_\mathrm{a}, n_\mathrm{h}\} \tag{4a}$$

$$\int_{\partial\Omega_\mathrm{coll.out}} r\rho\vec{u}(\vec{x})\,\mathrm{d}\vec{x} = S\left(\frac{\pi}{2} + \theta\right) \cdot \int_{\partial\Omega_\mathrm{chim.in}} r\rho\vec{u}(\vec{x})\,\mathrm{d}\vec{x}. \tag{4b}$$

$$\int_{\partial\Omega_\mathrm{coll.out}} rp(\vec{x})\,\mathrm{d}\vec{x} - A_\mathrm{coll.out}\Delta p = \int_{\partial\Omega_\mathrm{chim.in}} rp(\vec{x})\,\mathrm{d}\vec{x}. \tag{4c}$$

(4a) states that while the properties should be preserved overall, we do not attempt to construct a point-to-point map between collector exit and chimney entrance. In (4b), where S denotes a rotation matrix, we describe the air being guided from its motion parallel to the ground to vertical ascend. The pressure Eq. (4c) as well as the lack of a sink term in (4b) are due to the fact that the turbines used in SUTs are pressure-staged [47]. Note that instead of a pressure loss factor f the absolute pressure drop Δp is used in this model.

The SUT is coupled to its surroundings at $\partial\Omega_\mathrm{coll.in}$ and $\partial\Omega_\mathrm{chim.out}$ by the usual inflow conditions for ρ, n, and T, and Dirichlet boundary condition for p [25,39]:

$$p = p_\mathrm{ex} + \Delta p_\mathrm{wind} \tag{5a}$$

$$\rho = \rho_{\mathrm{ex}}, n = n_{\mathrm{ex}}, T = T_{\mathrm{ex}}, \text{ if } \quad \vec{u} \cdot \vec{n} > 0. \tag{5b}$$

The term $\Delta p_{\mathrm{wind}} = \Delta p_{\mathrm{wind}}(x, t)$ is introduced to account for a potentially higher or lower effective pressure due to ambient wind. Due to the assumed radial symmetry, this is only directly applicable to collector geometries in which the air can only enter in one direction, such as the described triangular sloped collector field. If this is not the case, our modeling approach allows to split the collector into sectors which could then be treated separately.

3.4. 1d model

In order to simplify our model, we now integrate over collector height and chimney radius. By doing this, boundary conditions (3a)–(3d) will be transformed to source terms. In the conservation of momentum (2c), the no-slip condition (3a) will be replaced by the well-known friction term $\xi u|u|$. To determine the mass flow J, follow [48]: First solve (3c) for $u_\perp$ and plug it into the analogous definition of J:

$$J_{\mathrm{h}} = -\Gamma\left(\frac{1}{1-\frac{n_{\mathrm{h}}}{n}}\right) n \frac{\partial}{\partial \vec{n}}\left(\frac{n_{\mathrm{h}}}{n}\right).$$

Assuming J to be constant over a thin boundary layer of thickness δ yields

$$J_{\mathrm{h}} = \frac{1}{\delta}\int_0^\delta J_{\mathrm{h}}\, \mathrm{d}x_\perp = -\frac{\Gamma n}{\delta}\int_0^\delta \left(\frac{1}{1-\frac{n_{\mathrm{h}}}{n}}\right)\frac{\partial}{\partial \vec{n}}\left(\frac{n_{\mathrm{h}}}{n}\right)\mathrm{d}x_\perp = \frac{\Gamma n}{\delta}\ln\left(\frac{1-\frac{n_{\mathrm{h}}(\delta)}{n}}{1-\frac{n_{\mathrm{h}}(0)}{n}}\right). \tag{6}$$

An expression for the energy source term

$$\Phi := \mathrm{c}_1 T J_{\mathrm{h}} - \frac{\mathrm{Re}}{\mathrm{Pr}}\frac{\partial T}{\partial \vec{n}} \tag{7}$$

in conservation law (2d) can be achieved in a similar manner: The ansatz $(\Phi)_{\vec{n}} = 0$ leads to

$$T = T(0) + (T(\delta) - T(0))\frac{\exp\left(\mathrm{c}_1 \frac{\mathrm{Pr}}{\mathrm{Re}} J_{\mathrm{h}} x_\perp\right) - 1}{\exp\left(\mathrm{c}_1 \frac{\mathrm{Pr}}{\mathrm{Re}} J_{\mathrm{h}} \delta\right) - 1}.$$

Evaluating Φ at $x_\perp = 0$ and $x_\perp = \delta$ yields the symmetric expression

$$\Phi = \mathrm{c}_1 J_{\mathrm{h}} \frac{T_0 + T_\delta}{2} - \mathrm{c}_1 J_{\mathrm{h}} \frac{T_\delta - T_0}{2}\frac{\exp\left(\mathrm{c}_1 \frac{\mathrm{Pr}}{\mathrm{Re}} J_{\mathrm{h}} \delta\right) + 1}{\exp\left(\mathrm{c}_1 \frac{\mathrm{Pr}}{\mathrm{Re}} J_{\mathrm{h}} \delta\right) - 1}. \tag{8}$$

The first term in (8) can be interpreted as energy carried by the mass flux J, whereas the second represents the heat transfer by convection which is augmented or obstructed by J via a factor of the shape $f(x) = \frac{x(\exp(x)+1)}{\exp(x)-1}$. Straightforward analysis shows that f has a removable singularity and nice asymptotic behavior:

$$f(x) = f(-x); \quad \lim_{x\to 0} f(x) = 2; \quad \lim_{x\to 0} f'(x) = 0; \quad \lim_{x\to\pm\infty} f(x) - |x| = 0. \tag{9}$$

Plug (3d) into (7):

$$0 = \Phi + J_{\mathrm{h}}\left(\frac{1}{\mathrm{Ja}} - \mathrm{c}_1 T_0\right) - \frac{\mathrm{Re}}{\mathrm{Pr}}\begin{cases}\alpha(T_{\mathrm{ex}} - T_0) & \text{on } \partial\Omega_{\mathrm{chim.wall}} \cup \partial\Omega_{\mathrm{coll.roof}}\\ Q\cos(\theta - \beta) & \text{on } \partial\Omega_{\mathrm{coll.ground}}\end{cases}. \tag{10}$$

For the collector roof and the chimney wall, (10) is equivalent to the corresponding equations presented in [45,48]; for the collector ground it can be viewed as a modified Penman equation [49]. The properties of Φ derived in (9) facilitate an asymptotic analysis of (10): While $|J_{\mathrm{h}}| \to 0$ implies

$$\Phi = \frac{\mathrm{Re}}{\mathrm{Pr}}\begin{cases}\alpha(T_{\mathrm{ex}} - T_0) & \text{on } \partial\Omega_{\mathrm{chim.wall}} \cup \partial\Omega_{\mathrm{coll.roof}}\\ Q\cos(\theta - \beta) & \text{on } \partial\Omega_{\mathrm{coll.ground}}\end{cases} \tag{11}$$

and

$$\frac{T_0 - T_\delta}{\delta} = \begin{cases}\alpha(T_{\mathrm{ex}} - T_0) & \text{on } \partial\Omega_{\mathrm{chim.wall}} \cup \partial\Omega_{\mathrm{coll.roof}}\\ Q\cos(\theta - \beta) & \text{on } \partial\Omega_{\mathrm{coll.ground}},\end{cases} \tag{12}$$

i.e. regular heat flow as in the dry scenario, for $|J_{\mathrm{h}}| \to \infty$ we get

$$\frac{1}{\mathrm{Ja}}\frac{\mathrm{Pr}}{\mathrm{Re}} J_{\mathrm{h}} = \begin{cases}\alpha(T_{\mathrm{ex}} - T_0) & \text{on } \partial\Omega_{\mathrm{chim.wall}} \cup \partial\Omega_{\mathrm{coll.roof}}\\ Q\cos(\theta - \beta) & \text{on } \partial\Omega_{\mathrm{coll.ground}},\end{cases} \tag{13}$$

where all energy exchange through surfaces is used for condensation heat.

The derivation of J and Φ was based on the assumption of wet surfaces in (3b), implying that evaporation is always possible. To avoid unrealistically high rates, introduce a scalar function $J_{\max}$ on the surfaces as an upper bound. $J_{\max}$ will usually be 0 on the walls and the roof, but can be positive for the collector ground in case water is provided constantly by appropriate irrigation[1]. This irrigation can be thought e.g. as coming from additional use of the collector for desalination or agriculture. In the latter case, water consumption is a cost factor so restriction of water access appears natural. If J exceeds $J_{\max}$, set $J := J_{\max}$, find the corresponding T_0 by solving (6), and solve (10) or (12) for Φ. This procedure allows us to determine the mass and energy source terms J_{w}, Φ_{w} from the chimney wall and the collector roof as well as J_{g}, Φ_{g} from the ground for any given state of n_{a}, n_{h}, T and p in the SUT. The effect of varying $J_{\max}$ will be studied in Section 5.6.

After integration, the Euler equations for collector and chimney are simplified respectively to become the non-conservative system

$$
\begin{aligned}
(n_{\mathrm{a}})_t + (n_{\mathrm{a}}u)_x &= -\frac{A_x}{A} n_{\mathrm{a}} u \\
(n_{\mathrm{h}})_t + (n_{\mathrm{h}}u)_x &= -\frac{A_x}{A} n_{\mathrm{h}} u + \Sigma_{\mathrm{surf}} \frac{L}{A} J \\
\rho(u_t + u u_x) + \frac{1}{\epsilon} p_x &= -u \Sigma_{\mathrm{surf}} \frac{L}{A} \frac{M_{\mathrm{h}}}{M_{\mathrm{a}}} J - \frac{A_x}{A} \rho u^2 + \frac{\rho}{\mathrm{Fr}^2} \sin\theta + \Sigma_{\mathrm{surf}} \frac{L}{A} \xi \rho u |u| \\
p_t + \gamma (p u)_x &= (\gamma - 1) u p_x - \epsilon(\gamma - 1) \left(u\, \Sigma_{\mathrm{surf}} \rho \frac{L}{A} \xi u |u| - \frac{u^2}{2} \Sigma_{\mathrm{surf}} \frac{L}{A} \frac{M_{\mathrm{h}}}{M_{\mathrm{a}}} J \right) \\
&\quad - \epsilon(\gamma - 1) \frac{1}{\mathrm{Fr}^2} \Sigma_{\mathrm{surf}} \frac{L}{A} \frac{M_{\mathrm{h}}}{M_{\mathrm{a}}} J - \frac{A_x}{A} c_4 u p + \Sigma_{\mathrm{surf}} \frac{L}{A} \Phi \\
p &= T(n_{\mathrm{a}} + n_{\mathrm{h}}).
\end{aligned}
\tag{14}
$$

Note that on the transition from 2d to 1d, h and r have been replaced by the new variable $x \in (x_{\mathrm{coll.in}}, x_{\mathrm{coll.out}}) \cup (x_{\mathrm{chim.in}}, x_{\mathrm{chim.out}})$. $A(x)$ and $L(x)$ denote the cross-sectional area and the surface length at position x, while Σ_{surf} is a reminder that the source terms (i.e. friction $\xi \rho u|u|$ and condensation/evaporation J) have to be evaluated and summated over the types of surfaces relevant at x.

The systems on the intervals are coupled by integrated versions of (4a)–(4c), where equality of the cross-sectional areas $A_{\mathrm{coll.out}} = A_{\mathrm{chim.in}}$, which can be achieved by slightly shifting the transition between collector and turbine section, allows for simplification:

$$
f(x_{\mathrm{coll.out}}) = f(x_{\mathrm{chim.in}}) \quad \forall f \in \{T, n_{\mathrm{h}}, n_{\mathrm{a}}, u\} \tag{15a}
$$

$$
p(x_{\mathrm{coll.out}}) - \Delta p = p(x_{\mathrm{chim.in}}) \tag{15b}
$$

(10) is used in order to determine T_{g} and T_{w} and the outer boundary conditions (5a) and (5b) are still valid.

3.5. Low Mach number asymptotics

After performing low Mach number asymptotics as in [25,39,50], the systems can in first order be approximated by:

$$
u(x) = \frac{A_{\mathrm{coll.out}}}{A(x)} u_{\mathrm{coll.out}} - \frac{1}{A(x)} \int_x^{x_{\mathrm{coll.out}}} \frac{L(y)}{c_4} (\Phi(T_{\mathrm{w}}) + \Phi(T_{\mathrm{g}}))\, \mathrm{d}y \tag{16a}
$$

$$
(n_{\mathrm{a}})_t + u (n_{\mathrm{a}})_x = -\frac{L(x)}{A(x)} \frac{n_L}{c_4} (\Phi(T_{\mathrm{w}}) + \Phi(T_{\mathrm{g}})) \tag{16b}
$$

$$
(n_{\mathrm{h}})_t + u (n_{\mathrm{h}})_x = \frac{L(x)}{A(x)} \left(J(T_{\mathrm{g}}) + J(T_{\mathrm{w}}) - \frac{n_{\mathrm{h}}}{c_4} (\Phi(T_{\mathrm{w}}) + \Phi(T_{\mathrm{g}})) \right) \tag{16c}
$$

$$
\begin{aligned}
(u_{\mathrm{t}})_t = -\frac{1}{\int_{\mathrm{coll}} \rho\, \mathrm{d}x + \int_{\mathrm{chim}} \rho\, \mathrm{d}x} & \left(\int_{\mathrm{coll}}^{\mathrm{chim}} \lambda \rho u |u| - \frac{\sin(\theta)}{\mathrm{Fr}^2} \left(\frac{\rho_{\mathrm{ex}}}{\rho} - 1 \right) + \rho u (u)_x \, \mathrm{d}x \right. \\
& + \int_{\mathrm{coll}} u c_2 \frac{L}{A} (J(T_{\mathrm{g}}) + T_{\mathrm{w}})) - \rho \left(\frac{1}{A} \int_x^{x_{\mathrm{coll.out}}} \frac{L}{c_4} (\Phi(T_{\mathrm{w}}) + \Phi(T_{\mathrm{g}}))\, \mathrm{d}y \right)_t \mathrm{d}x \\
& \left. + \int_{\mathrm{chim}} u c_2 \frac{L}{A} J(T_{\mathrm{w}}) - \rho \left(\frac{1}{A} \int_{x_{\mathrm{chim.in}}}^{x} \frac{L}{c_4} \Phi(T_{\mathrm{w}})\, \mathrm{d}y \right)_t \mathrm{d}x + \Delta p \right),
\end{aligned}
\tag{16d}
$$

[1] For brevity, we will also write $J_{\max} = y$, with $y \in \mathbb{R}^+$ denoting the constant rate of irrigation on the collector ground, or $J_{\max} = f(x)$ for sector-wise irrigation.

where

$$c_3 := \frac{c_1 n_h + n_a}{n}; \quad c_4 := \frac{\gamma + c_3 - 1}{c_3}.$$

For a chimney with constant radius[2], such as in the Manzanares prototype or the plants proposed by Bilgen and Rheault [1], (16a)–(16c) become

$$u(x) = u_t + \int_{x_{\text{chim.in}}}^{x} \frac{2}{r_{\text{chim}}} \frac{\Phi(T_w)}{c_4} \, dy. \tag{17a}$$

$$(n_a)_t + u(n_a)_x = -\frac{2}{r_{\text{chim}}} \frac{n_a}{c_4} \Phi(T_w) \tag{17b}$$

$$(n_h)_t + u(n_h)_x = \frac{2}{r_{\text{chim}}} \left(J(T_w) - \frac{n_h}{c_4} \Phi(T_w) \right). \tag{17c}$$

In (16d), the term $\int_{\text{coll}}^{\text{chim}} \frac{\sin(\theta)}{\text{Fr}^2} \left(\frac{\rho_{\text{ex}}}{\rho} - 1 \right) dx$ denotes the updraft, where integration over the collector can be omitted for the flat setup. The turbine pressure loss factor f, which is often employed as a means for plant operation control, describes the fraction of the updraft that is extracted for electrical energy production in the turbine and therefore cannot be used for acceleration of the air flow, i.e. we define

$$f := \frac{\Delta p}{\int_{\text{coll}}^{\text{chim}} \frac{\sin(\theta)}{\text{Fr}^2} \left(\frac{\rho_{\text{ex}}}{\rho} - 1 \right) dx}. \tag{18}$$

From the coupling conditions (15a), only

$$n_a(x_{\text{coll.out}}) = n_a(x_{\text{chim.in}}) \text{ and } n_h(x_{\text{coll.out}}) = n_h(x_{\text{chim.in}}) \tag{19}$$

are still relevant, (10) still applies. The initial conditions are taken first order in ε, too, which yields

$$\rho(0, x) = \rho_{\text{ex}} \equiv 1 \quad \text{and} \quad T(0, x) = T_{\text{ex}} \equiv 1 \tag{20}$$

in our scaling; note that the initial and boundary conditions on p still appear as part of (16d).

It is readily shown that for the dry case, i.e. $J_{\max} = 0$ and $(n_h)_{\text{ex}}$ sufficiently low so that no condensation occurs, the model simplifies to be very similar to [39].

3.6. Steady state

In steady state, where the time derivatives vanish, the system (16a)–(16d) becomes

$$u_x = \frac{1}{c_4} \Sigma_{\text{surf}} \frac{L}{A} \Phi - u \frac{A_x}{A} \tag{21a}$$

$$(n_a)_x = -\frac{1}{u} \frac{n_a}{c_4} \Sigma_{\text{surf}} \frac{L}{A} \Phi \tag{21b}$$

$$(n_h)_x = \frac{1}{u} \left(\Sigma_{\text{surf}} \frac{L}{A} J - \frac{n_h}{c_4} \Sigma_{\text{surf}} \frac{L}{A} \Phi \right) \tag{21c}$$

$$\Delta p = \int_0^1 -\Sigma_{\text{surf}} \frac{L}{A} \xi \rho u |u| - u \, \Sigma_{\text{surf}} \frac{L}{A} \frac{M_h}{M_a} J - \rho u u_x + \frac{\sin(\theta)}{\text{Fr}^2} (1 - \rho) \, dx. \tag{21d}$$

4. Numerical simulations

4.1. Algorithms

In this section, we discuss the numerical simulation and optimization of the transient model (16a)–(16d) and the steady-state model (21a)–(21d). Eqs. (16b), (16c) and (16d) from the last section are evolution equations. For the unknown $\rho(x, t)$ we have a transport partial differential equation (PDE) and for $v(t)$ we have an ordinary differential equation (ODE). Note that the boundary conditions for pressure and the turbine pressure drop (5a) and (15b) are already incorporated in (16d) as

[2] For non-constant radii $r_{\text{chim}} = r_{\text{chim}}(x)$, u_t in (17a) only gets an additional Bernoulli-like factor corresponding to the one in (16a)

Table 8
Comparison of simulation times for a run in dry air conditions (with fixed parameters).

Transient Simulation	Steady-state simulation	
	u_0 given	Δp given
0.64 s	0.60 s	12.7 s

Table 9
Comparison of simulation times for a steady state simulation for dry and wet conditions (with fixed parameters).

	Dry	Wet
u_0 given	0.60 s	0.64 s
Δp given	12.60 s	12.66 s

parameter. We have the boundary conditions (5b) for ρ and the initial conditions (20) for ρ and v. The following is a sketch of our numerical (explicit forward in time) strategy to solve the system (16a)–(16d):

1. Update u from v in (16a).
2. Make an explicit upwind scheme in the PDEs (16b), (16c) for n_{a}, n_{h}.
3. Make an explicit time step in the ODE (16d) for v.
4. Repeat 1.–3. until steady state is reached.

This is a very simple but reasonable algorithm. The stability is ensured by the Courant–Friedrichs–Lewy (CFL) condition. Note that the CFL condition does not imply very restrictive time steps since due to Eqs. (16b) and (16c) it depends only on the flow velocity. This is in contrast to a fully nonlinear fluid model (like (14)) where the time steps in the small Mach number regime become very restrictive since there the CFL condition is governed by the speed of sound. A more detailed analysis related to efficiency from a numerical point of view in a similar model can be found in [46]. Moreover, it is possible to define more sophisticated schemes as well but – as we will see – there seems to be no strong need.

In many situations only the steady state solution is of deeper interest. There is more than one reason for that. One is that the transient solutions in most of the realistic situations converge rapidly (order of magnitude is 10 min) to a stationary state. A second reason is that, under the assumptions made, the changes in time of the data (boundary condition, solar radiation rate etc.) are very slow over a typical 24 h cycle. Therefore it is a reasonable alternative to solve over a 24 h cycle a few stationary problems, instead of running a transient problem over such a long time period. On top of that, later on we will investigate qualitatively how variation in one parameter affects performance at a particular point in time while the other parameters are kept constant. The natural choice for this is to consider equilibrium solutions. Thus we have, as an alternative, a simple scheme to solve the steady-state system (21a)–(21d):

1. Make an initial guess for the velocity at the collector entrance u_0.
2. Integrate (21a)–(21c) with boundary condition $(n_{\mathrm{a}}^{\mathrm{ex}}, n_{\mathrm{h}}^{\mathrm{ex}}, u_0)$ over collector and chimney employing a standard Runge–Kutta-method.
3. Calculate the corresponding turbine pressure loss $\Delta p(u_0)$ from (21d).
4. To match a given turbine pressure loss $\Delta p'$, use an iterative solver on steps 2.-3. to find u_0 satisfying $\Delta p(u_0) - \Delta p' = 0$.

In the following we will use in a few examples both the long time transient and the stationary approach to obtain the stationary solution. We will see that the two approaches lead – as expected – to the same result. Representative computation times on a PC (Intel (R) Core(TM) i5-2400 CPU @ 3.10 GHz, 8 GB memory) are given in Tables 8 and 9.

In the application optimization is an important issue. Therefore in a second step we would like to optimize. For the optimization of the power output we use

1.–4. Run transient simulation from former algorithm to obtain corresponding turbine velocity $u_{\mathrm{turb}}(\Delta p)$ for given turbine pressure loss Δp

5. Use standard Matlab optimization tool `fminsearch` on 1.–4. to find $\min\limits_{\Delta p>0} (-u_{\mathrm{turb}}(\Delta p) \cdot \Delta p)$.

Again, as an alternative (and as a crosscheck) for finding the optimal turbine pressure loss we can use a slightly changed approach:

1. Make an initial guess for velocity at collector entrance u_0.

2.-3. Find the turbine pressure loss $\Delta p(u_0)$ to the given initial velocity u_0 as before.

4. Use standard Matlab optimization tool `fminsearch` on 2.-3. to find $\min\limits_{u_0>0} (-u_{\mathrm{turb}} \cdot \Delta p(u_0))$.

Table 10
Simulation time for the optimization of the Power P as function of the control parameter f (Fig. 5).

Transient	Steady state
ca. 148 s	23 s

Table 11
Parameter values for geometry and environment of the simulated plants.

Parameter	Manzanares	Winnipeg
L_{coll}	120 m	1380 m
H_{chim}	200 m	60 m
h_{coll}	2 m	5 m
D_{chim}	10 m	54 m
Slope θ	0°	45.1°
Inclination β	39°	49.9°
Average temperature T_{ex}	27°C	3°C
Average relative humidity	57%	61%

Table 12
Parameter values used for all simulations.

Parameter	Value
α	10
ξ	0.1
p_{ex}	101328 Pa
Δp_{wind}	0 Pa
q	300 W

Note that both steady-state algorithms include an optimization. Therefore, finding the optimal pressure loss is not more expensive than calculating the steady state for a given pressure loss: both only involve a simple iteration of the integration of a first-order ODE system. Representative calculation times obtained for the optimization of the pressure loss factor are summarized in Table 10.

The most time consuming part of the simulation is the solution of the nonlinear surface energy balance (10) which has to be obtained at every grid point. This means that a significant speedup can be achieved where the asymptotic behavior in (11)–(13) can be used for direct calculation of the source terms, i.e. especially in the classical arid scenario.

4.2. Basic simulations

To verify the simplified model (16a)–(16d) s.t. (5b), (20) here we focus first on the direct simulation. As an example with flat collector we use the example of Manzanares where good experimental data is available [16].

In the case of sloped collectors and for the case of humidity, the situation is worse. The only reference with some simulations for solar updraft towers with sloped collectors is [1], the case of humidity is treated in [7,11]. But in both cases only long term simulations for some overall variables are presented such that direct comparisons for short term scenarios (or parameter optimizations) are not possible.

In the following we show two examples where we use the data in Tables 11 and 12. The examples are the already mentioned Manzanares SUT with flat collector and a potential SUT for high latitude with sloped collector in Winnipeg proposed by [1]. We note that the Manzanares SUT is the only example where we have real data. The geometrical data are given in Table 11. For simplicity in both cases we use a mean annual temperature and a mean annual humidity for the corresponding location given also in Table 11. Similar for the external pressure (both SUT's are at about sea level so it appears reasonable to apply the same pressure profile for simplicity and comparability) and the overall solar radiation. The initial conditions are obtained by inserting T_{ex} and p_{ex} into the small Mach number limit (20) of the adiabatic profiles. Also, to compare the cases we use the same friction and heat loss parameters for all the cases (see Table 12). These two parameters are a reasonable choice which guarantees that we can reproduce the existing real data of the Manzanares case by our model (see also [39]). In the sloped case – as in [1] – a triangular collector is considered, with triangle basis length $A(x_{coll.in})/h_{coll}$ equal to the triangle height L_{coll} (see Fig. 1(b)). An exception is made for h_{coll} i.e. the height of the glass roof above the ground in the collector section. For h_{coll} we considered a (constant) average value of 5 m whereas in [1] a gradually increasing value from 1.7 m at the collector entrance up to 10 m at the turbine was used. This approximation does not cause significant qualitative or quantitative changes in our analysis. Moreover, it seems more plausible from a design point of view to take h_{coll} constant [32,39,51].

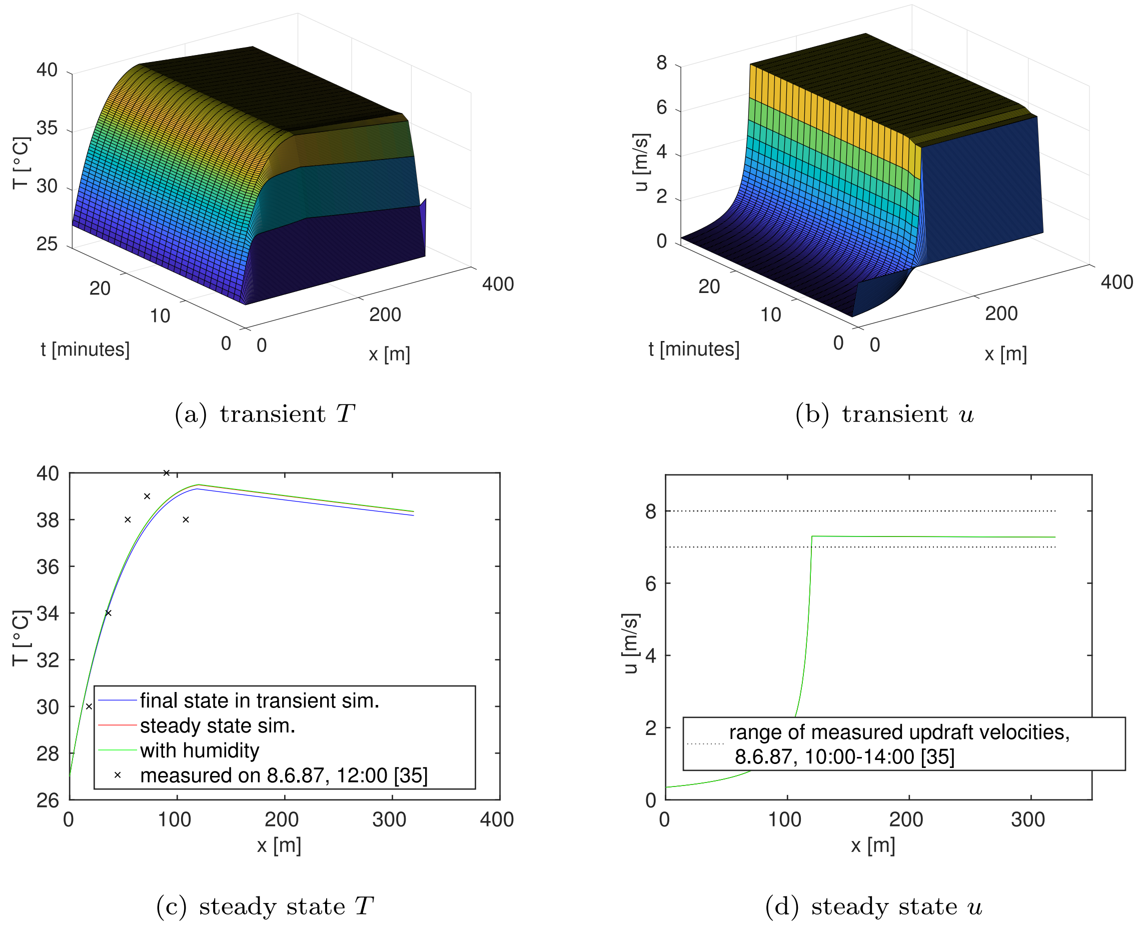

Fig. 3. Example of transient and steady state simulation for Manzanares and comparison with measurement data from [35] for validation.

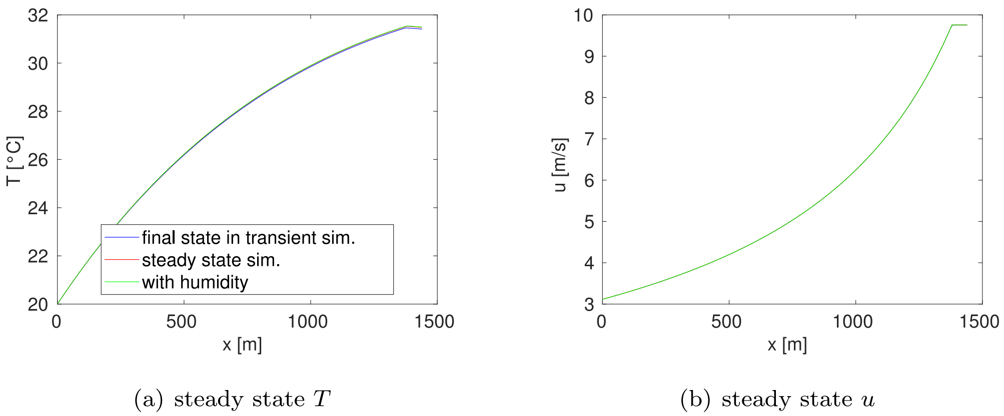

Fig. 4. Comparison between transient and steady state simulations (dry and wet) for Winnipeg.

The results of the simulations can be seen in Figs. 3 and 4, respectively. In Fig. 3 we start with two transient pictures for temperature and velocity to get an idea of the time evolution. We see that after a short period of about 10 – 20 min a stationary state is reached. The resulting profiles for temperature and velocity show nonlinear behavior. The velocity increases in the collector because of two reasons: the cross sectional area is decreasing (linearly) and the heated air is expanding. In the chimney the velocity is constant. The temperature shows a monotone (nonlinear) increasing profile too, in the chimney there is no significant change in the temperature. We would like to underline that here – in contrary to

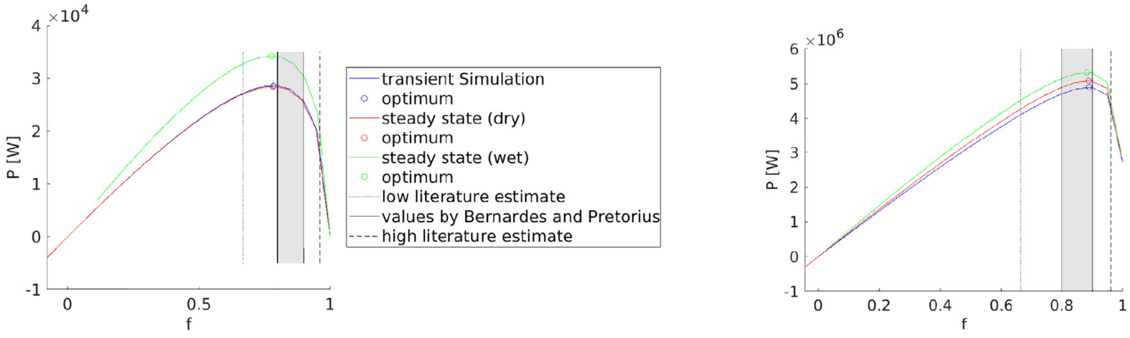

(a) Manzanares (b) Winnipeg

Fig. 5. Variation of pressure loss factor f for different locations and comparison with literature data for validation.

the Boussinesq approximation – there is no a priori assumption on a (linear) shape of the density or the temperature profile.

All the remaining results refer to the long time stationary case for temperature and velocity. In the Winnipeg example we show the stationary result obtained by the two approaches explained above, a long time transient approach and a stationary approach (see Fig. 4). As before, we include both the dry and the humid case to see the comparison. Note that here in these first examples for simplicity we assume no pressure loss in the turbine (i.e. no energy production). Nevertheless, we note that humidity in these cases has no influence on the performance.

In the next section besides the qualitative (and quantitative) understanding of the various temperature and velocity profiles, the main objective is to study the dependence of the main quantities – velocity and power – on the various parameters of the model.

5. Optimization

Here we present first results on optimizing with respect to certain parameters. The key quantity to be optimized is the power output. We aim to maximize the power output with respect to the optimal pressure loss factor, an optimal geometry, the optimal inclination of the collector, and optimality related to humidity. The pressure loss factor is an operational parameter (turbine control). Geometry and inclination are system parameters and relevant in the planning phase. Humidity can partly be influenced by water under the collector. Unfortunately, as in the previous section, there are no previous simulation results in the literature to compare our results with. However, in many cases the qualitative answer is reasonable. The simulations allow for identifying quantitatively the optimal values. This is in fact the advantage of our approach, to obtain rapidly reliable results in both the planning phase of a power plant and the operational phase of an existing power plant.

5.1. Optimal pressure loss factor for different heat losses

An interesting and important optimization parameter in the operational phase is the ratio of pressure loss at the turbine to the total pressure potential. If there is no pressure loss at the turbine – i.e. “extracting” no power – the highest possible velocity is reached. If we increase the pressure loss the air velocity becomes smaller and goes to zero. Since the power output is given by $P = c\,\Delta p\, u_{\text{turb}}$, both extreme cases give zero power output. We expect a maximal power output somewhere in between the two extreme cases. There is only one estimate for the optimal $f = 2/3$ in the literature [32] (see also [36,52,53]), valid only for the case of no friction, no heat losses and some other additional assumptions.

The realistic and interesting case with general losses is not analytically solvable. Simulations in the literature [36] indicate for a specific setting a value $f \approx 0.96$ close to the limit $f = 1$.

In Fig. 5 we show the dependence of the power output P on f for all four locations (from the previous section) in both the dry and the wet case. As in the previous section we assume a mean annual temperature and mean annual humidity for the different locations. We see (in the dry case) that both the transient and the stationary approach give good agreement in the results. Note that the different power plants give different optimal f, all the values lie between $f \approx 0.8$ and $f = 1$, but not so close to $f = 1$. In addition we see that when extracting significant power the humidity becomes important: higher humidity gives higher power output. This relation was conjectured by Kröger and Blaine (see [7]), with our approach we can easily quantify the effect.

Note also that the absolute values of the optimal power for the Manzanares power plant have the right order of magnitude (Manzanares was a 50 kW power plant). The same holds for the conjectured power output of the Winnipeg plant [1] in the order of 3 MW.

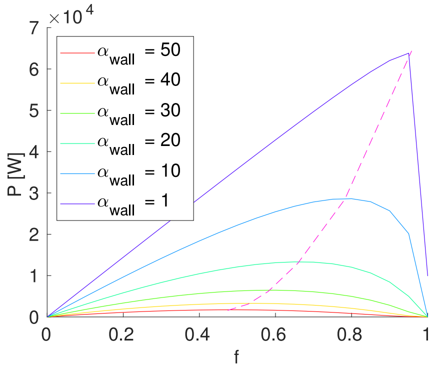

(a) Power output depending on pressure loss factor for different heat loss factor

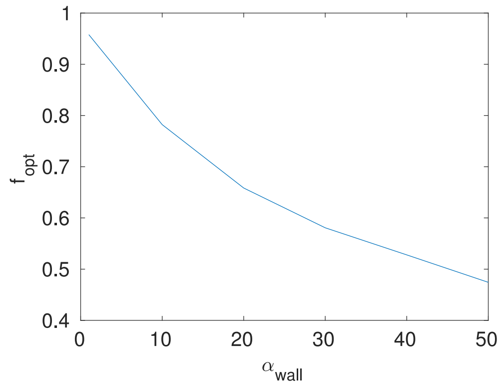

(b) Optimal pressure loss in dependence of heat loss factor

Fig. 6. Results for variable α_{wall}.

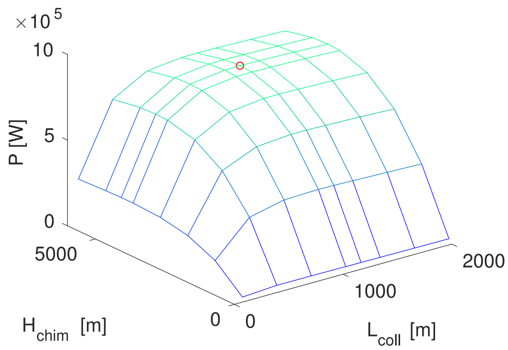

Fig. 7. Simultaneous variation of collector radius and chimney height with fixed collector height and chimney radius.

To further inquire the f dependence we look at the dependence of P on f for different values of the heat loss parameter (see Fig. 6). This gives interesting insight and shows that the optimal f increases with decreasing heat loss parameter α. And clearly, the higher the losses the lower the optimal power output (see Fig. 6 b)).

5.2. Plant geometry

In the planning phase one may ask about the optimal relation between the various parameters such as collector radius, collector height, chimney height, chimney radius etc. In Fig. 7 we show as an example the relation between collector radius and chimney height. The collector radius is related to the needed ground area and the chimney height goes with significant financial costs. We keep the chimney radius fixed at 5 m and the collector height fixed at 2 m, as in the Manzanares case.

It is interesting to see, that there is an optimal value for both, the optimal collector radius and the chimney height. Both values remain theoretical because they are very high, the optimal collector radius at more than 1000 m, and the optimal chimney height a few thousands of meters.

5.3. Influence of solar radiation Q

Not surprisingly, the dependence of the power output on the solar radiation is monotone (see Fig. 8 (a)). It seems to be almost linear and we can deduce a quantitative relation, power increases with a factor $\approx \frac{4}{3}$ faster than the solar radiation. The temperature and velocity profile are given in Fig. 8 (b) and (c), respectively.

5.4. Optimal collector slope for different inclinations

The issue of varying the collector slope can be approached in different ways.

To test our approach we start with a simple theoretical example. We assume a given SUT (with fixed slope angle θ, collector and chimney values) and vary the geographical position, i.e. the latitude β. Then – increasing the β starting from $0°$ or low values – we increase the area exposed vertically to the radiation (by a factor $\frac{1}{\sin\beta}$) up to the slope angle θ,

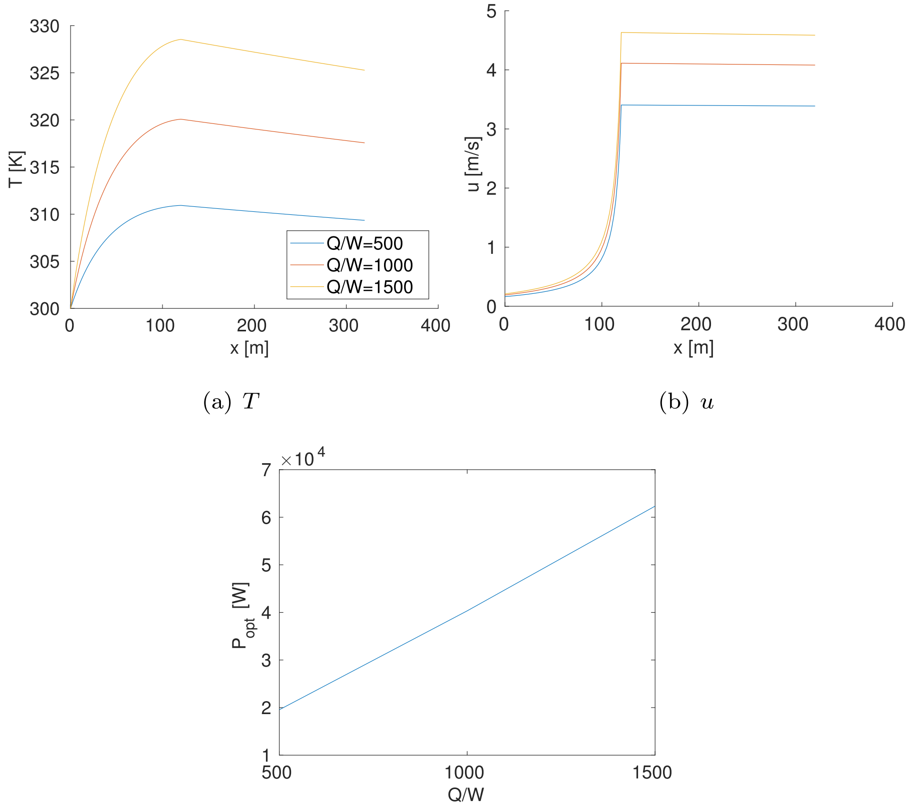

(a) T (b) u

(c) P

Fig. 8. Variation of solar radiation Q.

for further increase the vertically exposed area decreases again. Therefore the optimal β (or latitude for the given SUT) is expected to be the slope angle θ. In the Manzanares case with $\theta = 0^\circ$ we expect the optimal inclination to be $\beta = 0^\circ$, i.e. at the equator (Fig. 9 (a)). The green and red arrows in the inlays indicate the optimal and the real latitude, respectively. For the Winnipeg project with slope $\theta = 45.1^\circ$ the optimal latitude is exactly that value (see the result in Fig. 9 (b)).

Now we turn to a more realistic case. We fix the latitude β and vary only the slope of the collector θ. The collector length and the chimney height is taken fixed (the total height varies). Then with varying slope θ we expect two phenomena. First increasing θ the vertically exposed collector area increases up to $\theta = \beta$, for further increase the exposed area decreases again. The second effect is the chimney effect in the collector which increases monotonically with the slope θ. Therefore we expect the optimal value for θ to be higher than the latitude angle β. This is confirmed by the simulations and shown in Fig. 10. On the left we have the Manzanares example with $\beta = 39.9^\circ$ and an optimal slope angle of $\theta \approx 50^\circ$. On the right we have the Winnipeg example with $\beta = 49.9^\circ$ and an optimal slope angle of $\theta \approx 70^\circ$.

Finally we discuss an even more complex case. As before, we vary the slope and keep collector dimensions fixed. In addition we keep the total height of the power plant fixed, i.e. we vary the height of the chimney. Again we have two effects, the maximal exposure at the latitude angle $\theta = \beta$ and a varying chimney effect. The chimney effect increases because of the increasing slope of the collector but decreases because of the reduction of the chimney height. This possibly destroys the monotonicity. The result can be seen in Fig. 11, on the left for the Manzanares example, on the right for the Winnipeg example.

In summary we obtain an optimum for the Manzanares case at $\theta \approx 25^\circ < \beta = 39^\circ$. In the Winnipeg case above $\theta \approx 50^\circ$ we have no chimney left and the collector is cut off. However the optimal value is above that value.

This last example shows that such subtle dependencies are not always intuitively recognizable. However, with our model approach it is easy to describe and to quantify.

5.5. Influence of humidity without irrigation

Now we study a few examples considering humidity. First we only vary the relative humidity of the incoming air. In that case there are no evaporation and condensation phenomena to be expected in the power plant. In Fig. 12 we see higher

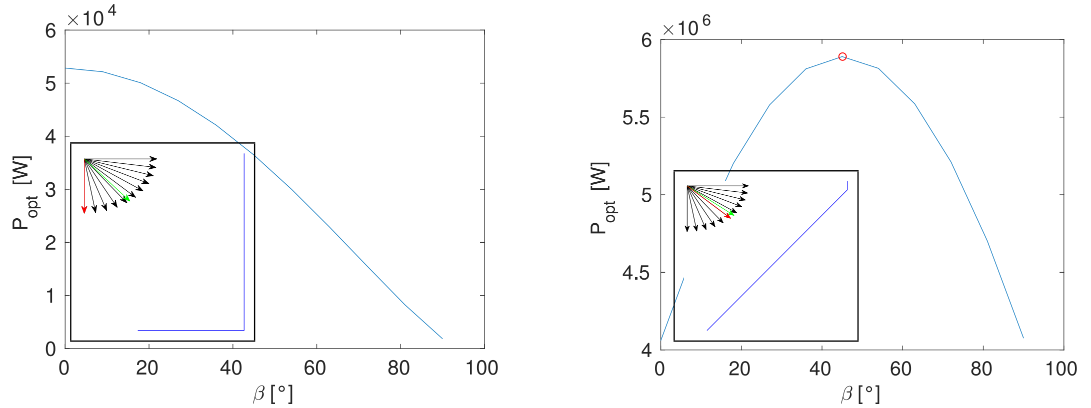

(a) Manzanares (collector slope $\theta = 0°$, latitude 39°)

(b) Winnipeg (collector slope $\theta = 45.1°$, latitude 49.9°)

Fig. 9. Varying the solar inclination β (latitude), and we obtain (as expected) $\beta_{opt} = \theta$. Insets: schematic view of SUP (green: normal inclination, red: optimal inclination). (For interpretation of the references to color in this figure legend, the reader is referred to the web version of this article.)

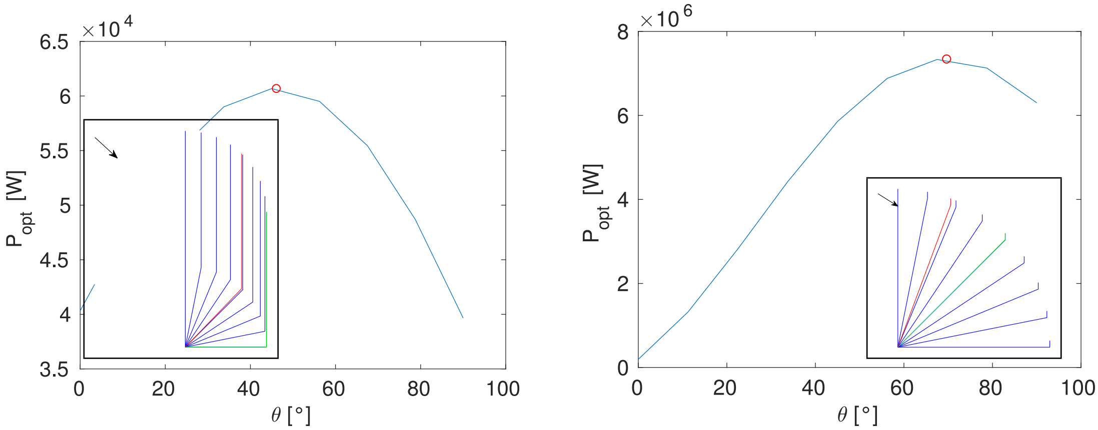

(a) Manzanares ($\beta = 39°$)

(b) Winnipeg ($\beta = 49.9°$)

Fig. 10. Varying collector slope with fixed chimney height gives optimal slope angles which are higher than the latitude. Insets: schematic view of SUP (green: normal slope, red: optimal slope). (For interpretation of the references to color in this figure legend, the reader is referred to the web version of this article.)

incoming humidity leads to lower temperatures, higher velocities and in particular to a higher heat capacity. In summary there is a weak dependence of the power on the incoming humidity. This was already conjectured by Kröger and Blaine [7].

5.6. Influence of maximal available irrigation

Finally we study the possibility of irrigation on the ground under the collector, e.g. from an additional agricultural usage. In this case potentially we have evaporation on the ground and an increase of humidity. This may induce condensation at the collector roof and at the chimney wall. In Fig. 13 (c) we see in detail the evaporation in the collector (solid lines) and the condensation at the collector roof and at the chimney wall (dashed lines). If there is a lot of water available (at the ground) both evaporation (only under the collector) and condensation takes place. The energy which is used for the evaporation is only partially recovered by condensation and in overall missing for heating and for the chimney effect. Therefore with increasing evaporation we expect decreasing power output. This can be seen in Fig. 13 (d). For higher evaporation we have lower temperatures (a) and lower velocities (b). This result is in agreement with the statement of Pretorius in [11] that a power reduction on the order of 50% has to be expected.

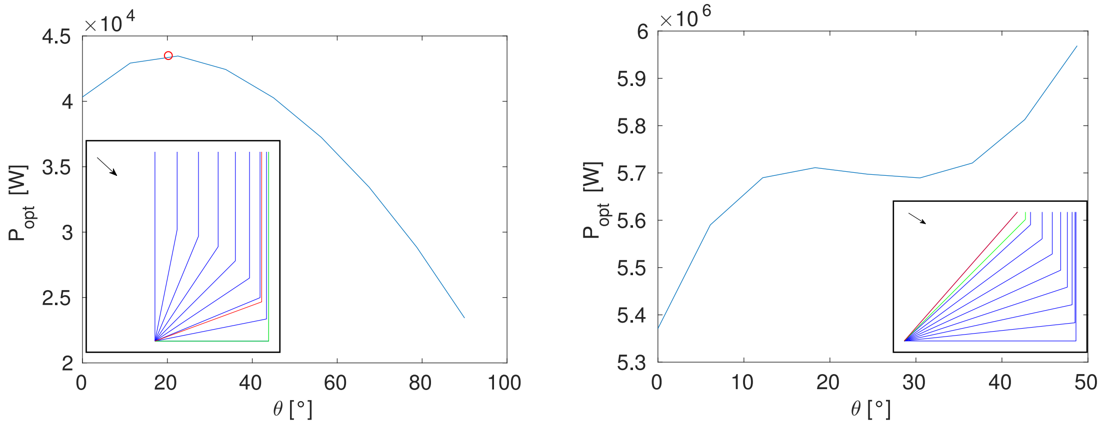

(a) Manzanares ($\beta = 39°$) (b) Winnipeg ($\beta = 49.9$)

Fig. 11. Varying collector slope with fixed overall height. Insets: schematic view of SUP (green: normal slope, red: optimal slope). (For interpretation of the references to color in this figure legend, the reader is referred to the web version of this article.)

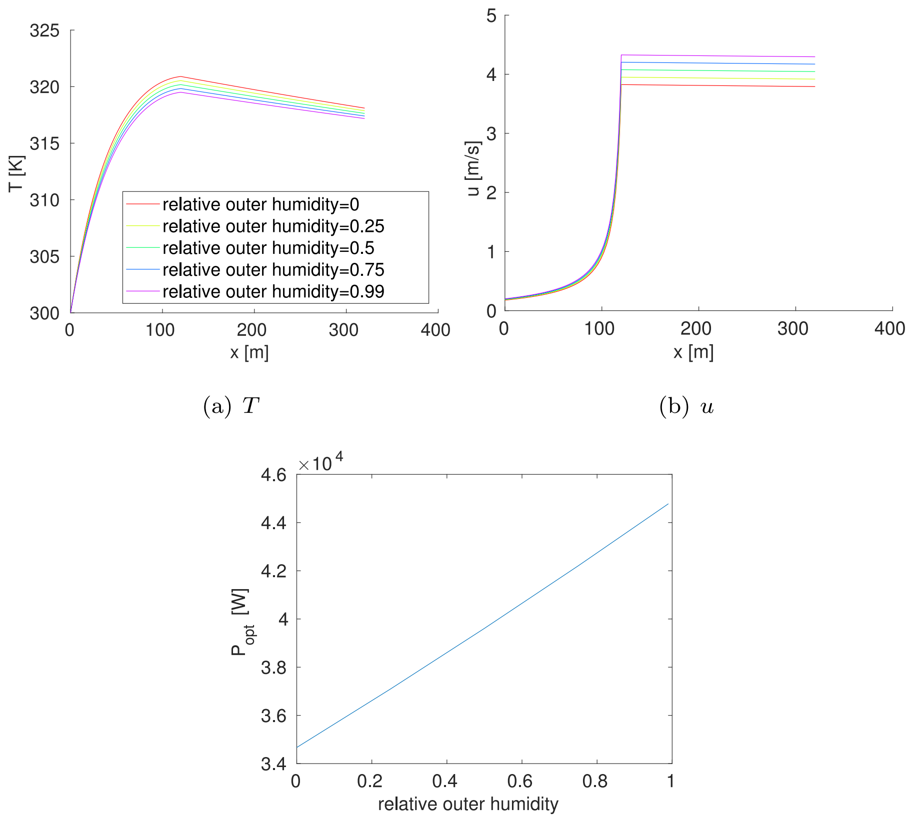

(a) T (b) u

(c) P

Fig. 12. Variation of outer humidity (Manzanares).

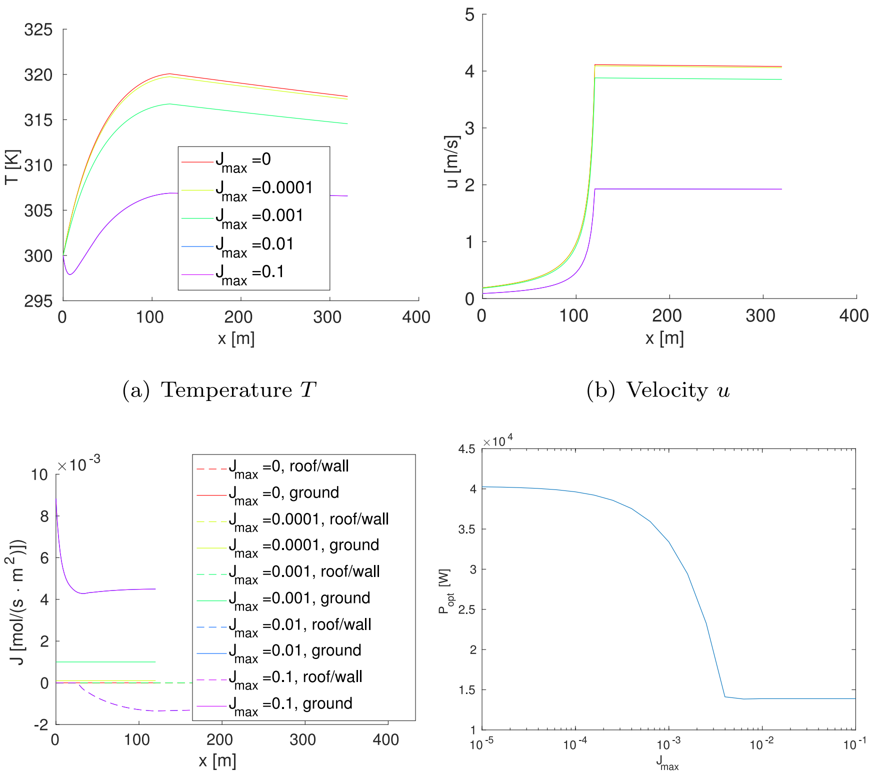

(a) Temperature T (b) Velocity u

(c) Condensation/evaporation J (d) Power output P on log scale

Fig. 13. Variation of maximal available irrigation J_{max} in the collector.

6. Conclusion

We present a one-dimensional asymptotic fluid dynamic model for the simulation of solar updraft towers with sloped collector which – according to [1] – are supposed to be much more efficient, in particular for higher latitudes. In addition the model describes the general case of humid air, whose influences on the performance of such thermo solar power stations was not clear up to now. The model describes the main physical effects and allows however – due to its simplicity – very fast simulations (much faster than real time). We confirm the results of [1] regarding the sloped collectors and re-discuss the results in [7,11] regarding the influence of the humidity. In addition the approach presented in this paper opens the possibility to optimize rapidly such a solar updraft tower with respect to parameters both in the planning and in the operational phase. This is of significant importance for the usability and the acceptance of such an alternative modeling and simulation approach.

More generally we can say that this is a valuable approach for general humid, buoyancy driven low Mach number flows. In such a highly complex “multi physics” context, one of the main challenges is a fast simulation of the direct problem in order to allow for optimization algorithms to be used on top. This is realised here in the context of a power station based on renewable solar energy.

References

[1] E. Bilgen, J. Rheault, Solar chimney power plants for high latitudes, Solar Energy 79 (5) (2005) 449–458.
[2] J. Schlaich, R. Bergermann, W. Schiel, G. Weinrebe, Design of commercial solar updraft tower systems—utilization of solar induced convective flows for power generation, J. Solar Energy Eng. 127 (1) (2005) 117–124.
[3] M. A. d. S. Bernardes, Solar Energy, InTech, 2010, Ch. Solar Chimney Power Plants - Developments and Advancements, pp. 171–186.
[4] S. Bernardes, M. Aurélio dos, Technische, ökonomische und ökologische Analyse von Aufwindkraftwerken, 2004.
[5] J. Schlaich, W. Schiel, Encyclopedia of Physical Science and Technology, third ed., Academic Press, London, 2001.
[6] G. Weinrebe, Das Aufwindkraftwerk Wasserkraftwerk der Wüste, Nova Acta Leopoldina NF 91 (339) (2004) 117–141.
[7] D. Kröger, D. Blaine, Analysis of the driving potential of a solar chimney power plant, R D J. 15 (3) (1999) 85–94.
[8] L. Zuo, Y. Zheng, Z. Li, Y. Sha, Solar chimneys integrated with sea water desalination, Desalination 276 (1–3) (2011) 207–213.
[9] L. Zuo, Y. Yuan, Z. Li, Y. Zheng, Experimental research on solar chimneys integrated with seawater desalination under practical weather condition, Desalination 298 (2012) 22–33.
[10] X. Zhou, B. Xiao, W. Liu, X. Guo, J. Yang, J. Fan, Comparison of classical solar chimney power system and combined solar chimney system for power generation and seawater desalination, Desalination 250 (1) (2010) 249–256.
[11] J.P. Pretorius, Optimization and Control of a Large-scale Solar Chimney Power Plant, University of Stellenbosch, Stellenbosch, 2007 Ph.D. thesis.

[12] I. Cabanyes, Proyecto de motor solar, La Energia Electrica 5 (4) (1903).
[13] D. Zaslavsky, R. Guetta, R. Hitron, G. Krivchenko, M. Burt, M. Poreh, Renewable resource hydro/aero-power generation plant and method of generating hydro/aero-power, 2003.
[14] H. Günther, In hundert Jahren : die künftige Energieversorgung der Welt, Franckh, Stuttgart, 1931.
[15] W. Haaf, K. Friedrich, G. Mayr, J. Schlaich, Solar chimneys part i: Principle and construction of the pilot plant in manzanares, Int. J. Sustain. Energy 2 (1) (1983) 3–20.
[16] W. Haaf, Solar chimneys part ii: Preliminary test results from the manzanares pilot plant, Int. J. Solar Energy 2 (2) (1984) 141–161.
[17] N. Pasumarthi, S.A. Sherif, Experimental and theoretical performance of a demonstration solar chimney model—part I: mathematical model development, Int. J. Energy Res. 22 (3) (1998) 277–288.
[18] N. Pasumarthi, S.A. Sherif, Experimental and theoretical performance of a demonstration solar chimney model–part II: experimental and theoretical results and economic analysis, Int. J. Energy Res. 22 (5) (1998) 443–461.
[19] J. Ruth, R. Gumpp (Eds.), Solar power plant. Studenten bauen das größte Aufwindkraftwerk Deutschlands, Bauhaus Universitätsverlag, 2009.
[20] F. Trieb, O. Langniß, H. Klaiß, Solar electricity generation–a comparative view of technologies, costs and environmental impact, Solar Energy 59 (1) (1997) 89–99.
[21] M.O. Hamdan, Analysis of a solar chimney power plant in the arabian gulf region, Renew. Energy 36 (10) (2011) 2593–2598.
[22] X. Zhou, Y. Xu, Solar updraft tower power generation, Solar Energy 128 (2014) 95–125.
[23] H.H. Al-Kayiem, O.C. Aja, Historic and recent progress in solar chimney power plant enhancing technologies, Renew. Sustain. Energy Rev. 58 (2016) 1269–1292.
[24] E. Lorenzo, De los archivos historicos de la energia solar: De una propuesta espanõla en 1903 a la Central de Manzanares, 2018 http://www.fotovoltaica.com/chimenea.pdf.
[25] M. Bauer, I. Gasser, Modeling, asymptotic analysis, and simulation of an energy tower, SIAM J. Appl. Math. 72 (1) (2012) 362–381.
[26] A.J. Gannon, T. von Backström, Solar chimney cycle analysis with system loss and solar collector performance, ASME J. Sol. Energy Eng. 122 (2000) 133–137.
[27] M.d.S. Bernardes, T. von Backström, D. Kröger, Analysis of some available heat transfer coefficients applicable to solar chimney power plant collectors, Solar Energy 83 (2009) 264–275.
[28] T. von Backström, Calculation of pressure and density in solar power plant chimneys, ASME J. Sol. Energy Eng. 125 (2003) 127–129.
[29] T. von Backström, A.J. Gannon, The solar chimney air standard thermodynamic cycle, S.A.I. MechE R D J. 16 (2000) 16–24.
[30] T. von Backström, T.P. Fluri, Compressible flow through solar power plant chimneys, ASME J. Sol. Energy Eng. 122 (2000) 138–145.
[31] M. Müller, Dreidimensionale Simulation der Strömungskontur eines Aufwindkraftwerkes, Studienarbeit, Inst. f. Strömungsmechanik und Hydr. Strömungsmaschinen, Univ. Stuttgart, 2002.
[32] G. Weinrebe, W. Schiel, Up-draught solar tower and down-draught energy tower - a comparison, in: Proceedings of the ISES Solar World Congress 2001, 2001.
[33] A. Koonsrisuk, T. Chitsomboon, A single dimensionless variable for solar chimney power plant modeling, Solar Energy 83 (12) (2009) 2136–2143.
[34] M.M. Padki, S.A. Sherif, On a simple analytical model for solar chimneys, Int. J. Energy Res. 23 (4) (1999) 345–349.
[35] B.J. Groenendaal, Solar Thermal Power Technologies. Monograph in the framework of the VLEEM Project, 2002.
[36] M.A.d.S. Bernardes, A. Voß, G. Weinrebe, Thermal and technical analyses of solar chimneys, Solar Energy 75 (6) (2003) 511–524.
[37] M. Tingzhen, L. Wei, X. Guoling, X. Yanbin, G. Xuhu, P. Yuan, Numerical simulation of the solar chimney power plant systems coupled with turbine, Renew. Energy 33 (5) (2008) 897–905.
[38] X. Zhou, J. Yang, B. Xiao, G. Hou, Simulation of a pilot solar chimney thermal power generating equipment, Renew. Energy 32 (10) (2007) 1637–1644.
[39] I. Gasser, Modelling and simulation of a solar updraft tower, Kinet. Rel. Models 2 (1) (2009) 191–204.
[40] J. Principe, R. Codina, Mathematical models for thermally coupled low speed flows, Adv. Theor. Appl. Anal. 2 (2009) 93–112.
[41] E. Felaco, I. Gasser, Modelling, asymptotic analysis and simulation of the gas dynamics in a chimney, J. Math. Ind. 3 (1) (2013) 1–20.
[42] T.M. VanReken, A. Nenes, Cloud formation in the plumes of solar chimney power generation facilities: a modeling study, J. Solar Energy Eng. 131 (1) (2009) 0110091–01100910.
[43] V.I. Khvorostyanov, J.A. Curry, Thermodynamics, Kinetics, and Microphysics of Clouds, Cambridge University Press, New York, NY, 2014.
[44] c. COSMO (Ed.), Core documentation of the COSMO-model, 2015, Last checked:1.8.2017. http://www.cosmo-model.org/content/model/documentation/core/default.htm.
[45] V. VDI (Ed.), VDI-Wärmeatlas, 10th Edition, Springer Vieweg, Berlin, Heidelberg, 2006.
[46] M. Rybicki, I. Gasser, Modelling and simulation of gas dynamics in an exhaust pipe, Appl. Math. Modell. 37 (5) (2013) 2747–2764.
[47] J. Schlaich, R. Bergermann, W. Schiel, G. Weinrebe, The Solar Updraft Tower : An Affordable and Inexhaustible Global Source of Electricity = Aufwindkraftwerke zur solaren Stromerzeugung, Bauwerk, Berlin, 2004.
[48] J.G. Collier, Convective Boiling and Condensation, second ed., McGraw-Hill, New York, 1981.
[49] J.L. Monteith, M.H. Unsworth, Principles of Environmental Physics, third ed., Elsevier/Acad. Press, Amsterdam, 2008.
[50] I. Gasser, J. Struckmeier, An asymptotic-induced one-dimensional model to describe fires in tunnels, Math. Methods Appl. Sci. 25 (14) (2002) 1231–1249.
[51] J. Schlaich, R. Bergermann, W. Schiel, G. Weinrebe, Design of commercial solar updraft tower systems - utilization of solar induced convective flows for power generation, J. Solar Energy Eng. 127(1) (2005) 117–124.
[52] M.A.d.S. Bernardes, T.W. von Backström, Evaluation of operational control strategies applicable to solar chimney power plants, Solar Energy 84 (2) (2010) 277–288.
[53] T.W. von Backström, T.P. Fluri, Maximum fluid power condition in solar chimney power plants an analytical approach, Solar Energy 80 (11) (2006) 1417–1423.